Electrochimica Acta, Vol. 36, No. 11/12, pp. 1775–1785, 1991
Printed in Great Britain.

0013-4686/91 $3.00 + 0.00

EXPERIMENTAL ASSESSMENT OF DYNAMIC STRUCTURAL PARAMETERS FOR HOMOGENEOUS AND INTERFACIAL CHARGE-TRANSFER REACTIONS: CASE STUDIES BASED ON TIME-DEPENDENT RAMAN SCATTERING METHODS

STEPHEN K. DOORN, ROBERT L. BLACKBOURN, CHRISTOPHER S. JOHNSON and JOSEPH T. HUPP
Department of Chemistry, Northwestern University, Evanston, IL 60208, U.S.A.

(*Received* 25 *February* 1991)

Abstract—The application of time-dependent scattering methodologies to dynamic structural problems involving charge transfer reactions is described. We show experimentally that a time-dependent analysis of resonance-enhanced Raman scattering can lead to a complete mode-by-mode description of the vibrational structural changes accompanying charge transfer and, therefore, a complete description of the vibrational activation barrier to charge transfer. (In other words, all force constants, all mode displacements, all bond-length displacements, and all individual energy components of the barrier can be determined.) The strategy is illustrated with case studies of internal (metal-to-ligand) charge transfer, ligand-bridged metal-to-metal charge transfer, outer-sphere charge transfer, and interfacial charge transfer.

Key words: Raman scattering, charge transfer, electron transfer.

INTRODUCTION

One of the key elements in any quantitative description of charge transfer reaction kinetics, in any environment, is an accurate estimate of internal (bond) reorganization effects[1–3]. These effects arise because of the oxidation-state dependence of the normal coordinates or internal bond lengths of redox-active molecular systems. Interconversion of oxidation states (charge transfer) therefore requires the displacement of coordinates (bond compression or bond stretching) and is generally accomplished by vibrational activation. The combination of net coordinate displacement and transient vibrational excitation leads to the familiar activation energy barrier diagram in Fig. 1. In this simple picture, the actual charge transfer occurs at the top of the barrier (the transition state) where the best compromise, in terms of bond lengths, has been achieved between the ground-state reactant and ground-state product. Alternatively, in a spectroscopic picture, the greatest vibrational overlap (largest Franck–Condon factor) is achieved at the top of the barrier. From Fermi's golden rule, the local charge-transfer probability will depend on the vibrational overlap squared. Provided that the activation process itself is not too costly, the actual charge transfer event again will occur at or near the top of the barrier. The interpretation of charge-transfer rates, therefore, becomes an exercise (in part) in the assessment of vibrational barriers.

For a thermoneutral reaction, *eg*

$$Fe(OH_2)_6^{3+} + Fe(OH_2)_6^{2+} \rightleftharpoons Fe(OH_2)_6^{2+} + Fe(OH_2)_6^{3+} \quad (1)$$

the vibrational barrier, ΔG_v^* can be readily calculated from a knowledge of unitless normal coordinate displacements (Δ_k) and vibrational frequencies (ν_k):

$$\Delta G_v^* = \frac{1}{8}\sum_k \Delta_k^2 \nu_k. \quad (2)$$

Alternatively, it can be obtained from values of bond displacements (Δa_j) and force constants (f_j) for bond activation:

$$\Delta G_v^* = \frac{1}{8}\sum_j b(\Delta a_j)^2 \nu_j^2. \quad (3)$$

In equation (3), b is the number of equivalent bonds displaced [for example, $b = 12$ for the Fe–O bond in equation (1)]. In both equations (2) and (3) the summation is over all modes or bonds displaced. To convert between the two equations, we require either: (a) a normal-coordinate analysis, so that mode displacements can be correctly partitioned among all the affected bonds, or (b) some form of local-mode approximation (*ie* a direct correspondence between particular modes and particular bonds). If the latter is acceptable, we obtain:

$$|\Delta a| = (\Delta^2 h/\mu\nu b)^{1/2} \quad (4)$$

$$f = 4\pi^2 \nu^2 c\mu. \quad (5)$$

In equations (4) and (5), h is Planck's constant, μ is a reduced mass, and c is the velocity of light.

If a net thermodynamic driving force (ΔG) exists, the effective barrier [ΔG^*(eff)] will be predictably modified[2]:

$$\Delta G^*(\text{eff}) = (2\,\Delta G^* + \Delta G)^2/4\,\Delta G^*. \quad (6)$$

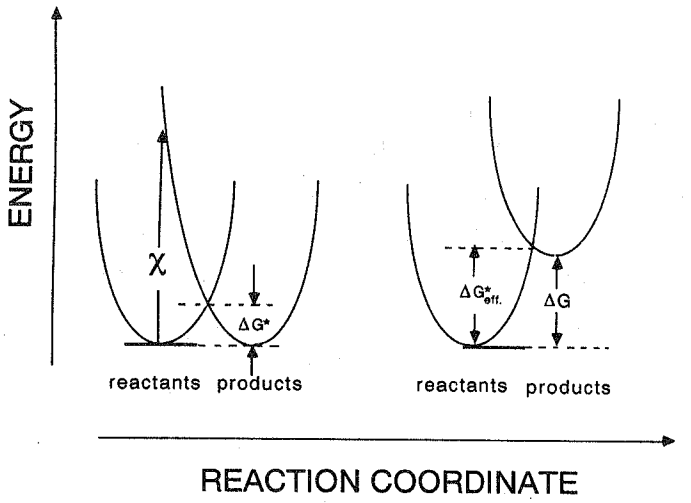

Fig. 1. Schematic representation of energy relationships for activated electron transfer in energy-neutral and endoergonic processes.

The form of equation (6) follows from the simplest of geometrical considerations (see Fig. 1) and is expected to hold whenever the reactant and product energy surfaces are parabolic, have similar curvature, and are not too strongly modified by the electronic coupling. One further point: equation (6) is written without subscript "v" so as to take account of not only vibrational activation but also solvent or other forms of activation which may sometimes contribute to observed kinetic barriers.

Given this simple theoretical treatment, the experimentalist's task is to obtain reliable estimates of force constants and bond or normal coordinate displacements and then to employ these to interpret or predict the effects of redox-induced structural changes upon charge-transfer reactivity. The most familiar approach, at least for thermal redox processes, has been to obtain estimates of Δa from X-ray structural studies of charge-transfer reactants and products in crystalline matrices and then to estimate force constants by some form of vibrational spectroscopy[3, 4]. This approach entails, of course, some skill in single-crystal growth and manipulation, and may therefore prove difficult for certain chemical systems. Perhaps more importantly, the crystallographic strategy assumes that parameters obtained in a structured solid are unperturbed upon immersion of a system in a solution or interfacial environment. We regard this assumption as particularly dangerous when strong molecule–solvent interactions exist, or in an electrochemical situation, when charge transfer is preceded by surface binding or specific adsorption.

An alternative method—solution (or interfacial) EXAFS—elegantly avoids these problems[4, 5]. Nevertheless, there still may exist difficulties. For example, EXAFS suffers from relatively poor precision (uncertainties of *ca* 0.01 Å are typically claimed for Δa in solution)[4] and a notable lack of sensitivity for selected elements and for most atoms remote from the scattering center. Furthermore, EXAFS methods, like X-ray crystallography, require that both halves of redox couple exhibit sustained chemical stability in order for Δa to be determined. This rules out, of course, any study of chemically irreversible reactions (for example, EC reactions where the C step entails product degradation) or any reaction involving rapid product-to-reactant relaxation (for example, allowed non-radiative decay following photo-excitation).

Given these limitations we have begun to explore an alternative approach to dynamic structure investigation. The method we have chosen is time-dependent Raman scattering[6–11]. This technique, while not really universal, is broadly applicable [10–21] and is highly complementary to traditional structural methods. The next section presents an abbreviated theoretical discussion of the scattering analysis. The remaining sections provide illustrative examples of its application to vibrational structural problems in homogeneous and interfacial charge-transfer environments.

TIME-DEPENDENT SCATTERING ANALYSIS

Recent theoretical[6–11] and experimental[10–21] efforts have convincingly shown that Raman scattering methods, especially time-dependent resonance methods, can yield very detailed information about dynamic structural changes. From a theoretical viewpoint, the time-dependent method has been largely developed and popularized by Heller and co-workers [6–8], although important contributions by Morris and Woodruff[9], Champion[11] and others should be noted. The historical basis for time-dependent theory development[7] was apparently in the more general realization that: (a) resonance vibrational spectroscopies are also electronic spectroscopies; (b) resonance spectra must contain, therefore, most or all of the information necessary to determine structural differences between resonant states; but (c) rigorous implementation of the necessary calculations would almost always prove impossible (due to the shear magnitude of the computation) if one employed the existing frequency-domain (sum-over-states) theoretical approach. The essence of Heller, Champion, Morris and Woodruff's work was to show that a half-Fourier transform to the time domain led to a tremendous

simplification of the conventional resonance Raman polarizability expression and therefore an enormous saving in computation time. Heller additionally implemented a semiclassical "wave packet" dynamics treatment which he used both to motivate and simplify the physical-chemical aspects of the scattering problem [6–8]. What follows in the remainder of this section is a primitive description of the time-dependent analysis, with primary emphasis on end results (*ie* analytically useful equations).

In the time-dependent picture of Raman scattering, electronic excitation to either a real (resonant) or virtual (non-resonant) upper state is also viewed as projecting a wave packet onto the real upper electronic surface[6–8]. Because the vibrational wave packet is not an eigenstate of the upper state, it evolves in time. Eventually, after an amount of time determined by the uncertainty principle (expressed in time–energy units) the system returns to the lower electronic surface and (simultaneously) scattering occurs. In energy terms, the scattering time is infinite (neglecting damping effects) when excitation occurs precisely at resonance, and essentially zero when excitation occurs far from resonance. (Thus the "time dependence" enters the problem in an analytical rather than experimental sense; the measurement itself is generally done in a steady-state fashion.)

As suggested in Fig. 2, the key theoretically to accomplishing efficient Raman scattering (electronic enhancement) is to achieve good overlap between the time-evolving (upper surface) initial state $[\phi_i(t)]$ and the vibrationally excited ($v = 1$; lower surface) final state (ϕ_f). At zero time the overlap is zero (note that a node exists for $v = 1$) and enhancement is absent. As the wave packet moves, however, the overlap builds up and scattering is enhanced. The extent to which the packet moves (prior to scattering) is determined by how closely one approaches resonance. A simple mathematical summary is the following[6]:

$$\alpha_{fi}(\omega_l) = \text{constant} \times \int_0^\infty e^{i\Delta\omega - \Gamma t} \langle \phi_f | \phi_i(t) \rangle \, dt. \quad (7)$$

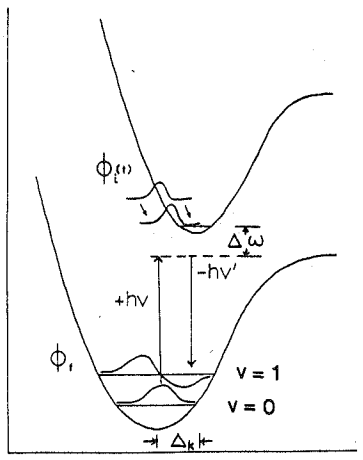

Fig. 2. Simplified depiction of time-dependent analysis of Raman scattering. $\Delta\omega$ is the energy mismatch between the virtual excited state and the real excited-state potential surface. $\phi_i(t)$ is the initial wave packet propagated in time on the upper surface. Its time-dependent overlap with ϕ_f, the vibrationally excited state of ground electronic surfaces, defines the Raman polarizability.

In equation (7), α_{fi} is the Raman polarizability tensor, $\Delta\omega$ is the difference between the incident frequency (ω_l) and the frequency of the resonant electronic transition, Γ is a damping factor, i denotes a complex number, f and i (subscripts) signify initial and final parameters, and t is time.

Structural information is obtained from this analysis by noting: (1) that the overlap at any specified time, for any specified mode, depends on the relative steepness of the upper potential energy surface and its "horizontal" displacement from the lower one; and (2) that the scattering intensity for any particular mode is proportional to the polarizability squared. Since, for any particular mode, the surface steepness and upper/lower horizontal displacement define the vibrational force constant and unitless coordinate displacement (Δ), respectively, there is an opportunity to extract these quantities from relative Raman intensity measurements under conditions of resonance enhancement. The key equation derived by Tannor and Heller[6] is

$$\frac{I_1}{I_2} = \frac{\omega_{1e}^2 \Delta_1^2 \omega_{2g}}{\omega_{2e}^3 \Delta_2^2 \omega_{1g}}. \quad (8)$$

In equation (8), I_1 and I_2 are scattered Raman intensities from modes 1 and 2, ω is 2π times the vibrationally frequency (ν), and the indices e and g designate the excited- and ground-state potential surfaces, respectively. If there are no changes in vibrational frequencies upon electronic excitation, or if the changes are sufficiently small to be neglected, equation (9) can be simplified[6]:

$$\frac{I_1}{I_2} = \frac{\Delta_1^2 \omega_1^2}{\Delta_2^2 \omega_2^2}. \quad (9)$$

In equation (9), ω now refers to ground-state frequencies. Equations (8) and (9) yield relative normal coordinate displacements; absolute scaling is available from[6]

$$2\sigma^2 = \sum_k \Delta_k^2 \nu_k^2, \quad (10)$$

where $8\sigma^2$ is the square of the electronic absorption band width at 1/e of the height, and the summation is over all modes that show significant intensity in the Raman spectrum. Finally, equation (4) permits Δ values to be converted to absolute bond distortions ($|\Delta a|$) in those cases where a local mode approximation is appropriate.

To relate the structural parameters to activation energies we first note that it is customary to express ΔG^* values in terms of vertical reorganization energies (χ; Fig. 1):

$$4\,\Delta G^* = \chi, \quad (11)$$

where ΔG^* is the activation free energy in the absence of a driving force component. With this definition [equations (2), (3) and (11)], χ is given vibrationally by:

$$\chi_v = (1/2) \sum_k \Delta_k^2 \nu_k = (1/2) \sum_j b_j (\Delta a)_j^2 f_j. \quad (12)$$

Likewise, individual normal coordinate contributions (χ_v) are given by:

$$\chi_v = (1/2)\,\Delta^2 \nu. \quad (13)$$

Thus the scattering analysis provides a means for determining all normal coordinate displacements, all bond displacements, all force constants, and all individual components of the vibrational reorganization energy for a given electronic transition.

Equations (12) and (13) are universally applicable. The scattering analysis itself, however, is strictly applicable only when: (1) mode-mixing (Duschinsky rotation) is absent[9]; (2) Herzberg–Teller coupling to higher electronic excited states is absent[17]; (3) only a single electronic transition is in resonance or near resonance[17]; (4) only ground vibrational states of the ground electronic state are populated[22]; and (5) scattering occurs under "short time" conditions[6–8]. Deviations from the first four conditions have been described elsewhere[9, 17, 22] and can be handled computationally with more complex analytical or numerical expressions. The fifth condition has also been described[6–8], but merits further explanation. In the wave packet analysis, the term short-time dynamics refers to scattering which arises from an initial overlap that decays rapidly and does not recur. In other words, it refers to scattering which occurs when the wave packet has completely transversed the upper surface less than once. Experimentally, the short-time condition can be fulfilled either by exciting at preresonance or by investigating systems with sufficient numbers of modes that damping effects prevent recursion. For all of the systems we have investigated thus far, the second effect has been found to be sufficient. As a practical matter, this means that the scattering analysis can be applied both at resonance and preresonance. Nevertheless, it should be kept in mind when investigating new systems (especially small systems) that the methodology is not necessarily always applicable to experiments done at resonance.

METAL-TO-LIGAND CHARGE TRANSFER

Among the simplest and most common of electron transfer reactions are internal charge transfers such as metal-to-ligand or ligand-to-metal charge transfer. These types of reactions have attracted considerable attention over the last 15 years because of their potential use in molecule-based solar energy conversion schemes[23]. Among the issues in energy applications are photo-stability, efficiency of light collection, and length of photo-excited state (charge transfer state) lifetime. One of the primary factors determining the lifetime is the rate of non-radiative decay, which in turn depends on: (1) the magnitude of the ground-state/excited-state energy gap; and (2) the magnitude of normal coordinate displacements—especially displacements associated with high-frequency energy-accepting modes[23–25]. Since the mechanism of non-radiative decay is generally charge recombination, the lifetime problem is basically an exothermic electron transfer problem. We note further that from a structural viewpoint, MLCT excitation and non-radiative decay are forward and reverse versions of the same net chemical reaction; accordingly, information collected about one may be directly applicable to the other.

As an example of time-dependent analysis, we recently reported on the vibrational structural changes accompanying metal-to-ligand charge transfer

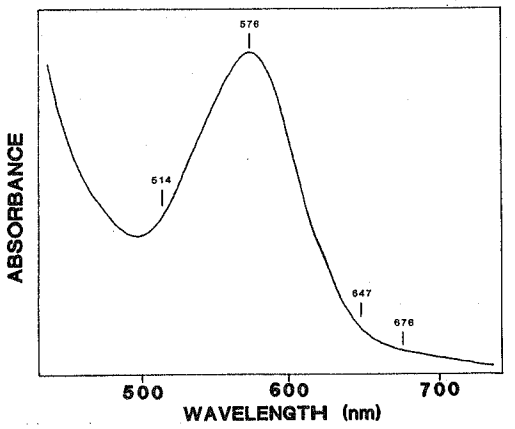

Fig. 3. MLCT absorption spectrum of $Ru(HN_3)_4(bpy)^{2+}$ in hexamethylphosphoramide as solvent (from Ref.[18]).

(MLCT) in $Ru(NH_3)_4(bpy)^{2+}$ (bpy is 2,2′bipyridine) [18]:

$$Ru^{II}(NH_3)_4(bpy)^{2+} \xrightarrow{h\nu} Ru^{III}(NH_3)_4(bpy^-)^{2+}. \quad (14)$$

This species was chosen because it is strongly chromophoric, reasonably photo-stable, and completely non-luminescent. In addition, because the complex contains 12 potential hydrogen bonding sites (in the form of ammine protons) the MLCT energetics are exceedingly sensitive to the nature of the solvent. One might expect, therefore, to be able to test current ideas about how internal (vibrational) reorganization is influenced by strong external (solvent/ligand) interactions.

Figure 3 shows a visible region absorption spectrum for $Ru(NH_3)_4(bpy)^{2+}$; the single peak centered at 576 nm corresponds to equation (14). Preresonant excitation at 647 nm (Kr^+ source) leads to the scattering spectrum shown in Fig. 4 and Table 1. Comparisons of intensities at 647 nm with those obtained at 676 nm (*ie* further from resonance) indicate that the

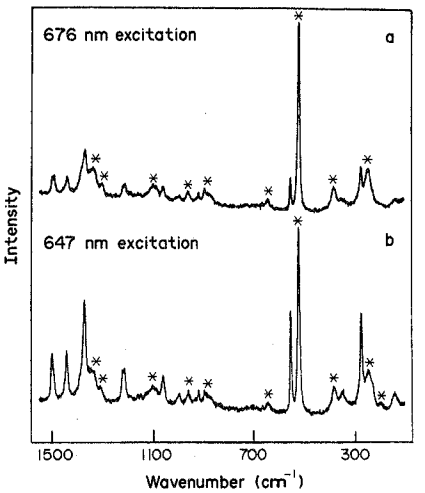

Fig. 4. Raman spectra of 50 mM $Ru(NH_3)_4(bpy)^{2+}$ in hexamethylphosphoramide as solvent. Excitation wavelengths: (a) 676 nm; (b) 647 nm. Solvent peaks are marked by asterisks.

Table 1. Vibrational assignments, scattering intensities, displacement parameters and MLCT reorganization energies for individual modes within $Ru(NH_3)_4(bpy)^{2+}$

Mode/ cm^{-1}	Relative intensity	Δ	χ_i/cm^{-1}	Primary assignment
1605	1	0.36	100	$\nu_{C=C}$
1548	0.96	0.36	100	$\nu_{C=C}$
1481	1.8	0.52	200	$\nu_{C=C}$
1331	0.66	0.35	82	$\nu_{C=N}$
1266	0.10	0.14	13	$\nu_{C=N}$
1250	0.10	0.15	14	$\nu_{C=C}$ inter-ring
1172	0.52	0.35	75	δ_{CCH} in plane
1106	0.24	0.26	36	δ_{CCH} in plane
1027	0.27	0.29	43	Ring breathing
767	0.12	0.26	26	δ_{CCH} out of plane
667	2.1	1.2	520	δ_{CCC} inter-ring
456	0.27	0.65	96	ν_{Ru-NH_3}
376	1.8	2.0	780	ν_{Ru-N}(bpy)
248	0.30	1.3	200	$\delta_{H_3N-Ru-NH_3}$

scattering at the shorter wavelength is resonantly enhanced (see Fig. 4).

The observation of resonance enhancement is significant because it implies that the time-dependent analysis can be utilized. It also implies that a very large number of modes are involved in vibrational activation (since a large number are electronically enhanced). Input of corrected intensities and vibrational frequencies leads to the Δ values listed in Table 1. (Also shown are χ_i' values for each mode.) For the low frequency (metal–ligand stretching) modes, individual Δ values can be further identified with individual bonds and therefore Δa values can be obtained. (For example, in Table 1, $|\Delta a|$ is determined to be 0.022 Å for each of the ruthenium–ammonia bonds.) On the other hand, for the higher frequency modes the unitless displacements are distributed over several different types of bond. Similarly, each ground-state/excited-state bond displacement involves contributions from multiple normal coordinates. Consequently, individual Δa values are not readily obtained. (If Δa values are needed, a full normal coordinate analysis is required.) Nevertheless, we[18] and others[26] have shown that composite estimates of ground-state/excited-state bond length changes (Δr)

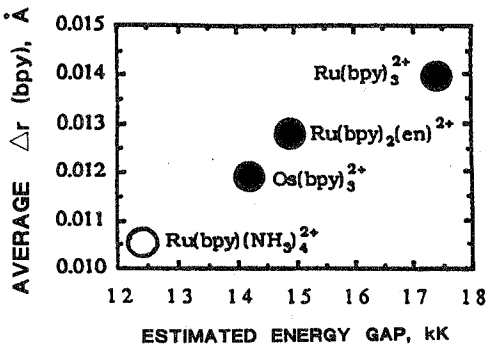

Fig. 5. Composite bpy framework bond displacements following MLCT excitation. Filled circles: values determined by application of Badger's rule to ground and excited state vibrational spectra (see Refs[26] and[18]). Open circle: value obtained from a weighted sum of normal coordinate displacements determined *via* time-dependent Raman scattering (see Ref.[26]).

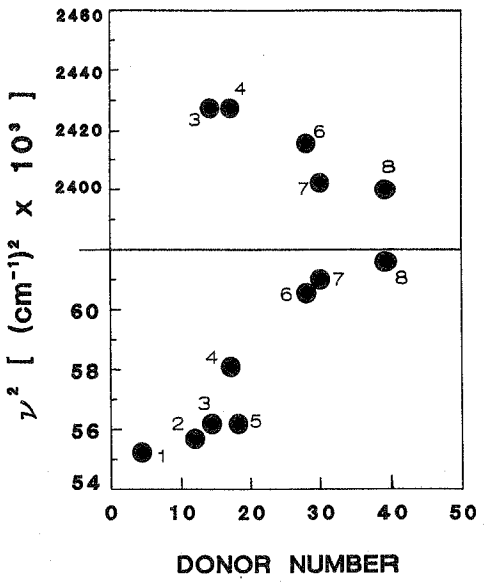

Fig. 6. Relative force constants (as measured by ν^2) for ν(C=C) (top panel) and $\delta(H_3N-Ru-NH_3)$ (bottom panel) within $Ru(NH_3)_4(bpy)^{2+}$, as a function of solvent basicity. Key to solvent: (1) nitrobenzene; (2) benzonitrile; (3) acetonitrile; (4) acetone; (5) H_2O; (6) dimethylacetamide; (7) dimethylsulfoxide; and (8) hexamethylphosphoramide.

can sometimes be obtained. For the 13 bipyridine-based C–C and C–N bonds, this entails an appropriate averaging of displacements for the six highest-frequency normal modes (*ie* the modes associated with distortion of the bpy rings). The value obtained for $Ru(NH_3)_4bpy^{2+}$ is 0.0106 Å.

It is worth noting that Δr values have been determined independently for three other transition-metal/bipyridine complexes[18, 26]; the method used was an empirical "Badger's rule" (frequency shift) correlation [18, 26, 27]. Figure 5 shows that there is reasonable agreement between these values and the value obtained from time-dependent scattering. Taken together with the $Ru-NH_3$ data and other results described in Ref. [18], we conclude that the preceding scattering experiments and analysis display a reasonable accuracy for dynamic structural determinations.

As noted above, solvent effects upon vibrational reorganization might be expected for $Ru(NH_3)_4(bpy)^{2+}$. One way of detecting these would be to observe vibrational frequency shifts as a function of solvent composition. We have done this for three of the enhanced modes in $Ru(NH_3)_4(bpy)^{2+}$; two are presented in Fig. 6[18]. The plots actually consist of ν^2 (essentially the vibrational force constant) *vs* the so-called solvent "donor number"[28]. The latter is, paradoxically, an empirical measure of the solvent's hydrogen-bond *accepting* (or electron-pair donating) ability. In any case, good correlations exist with ν^2.

For the lower frequency mode in Fig. 6 (an $H_3N-Ru-NH_3$ bend) the explanation proposed[18] for the solvent effect is first that the electron-deficient hydrogens on the ammonias can bind to electron-rich solvent functionalities. It follows that creation of a hydrogen bond in this way should lead ultimately to an increase in electron density at the metal center, and a strengthening of the metal–nitrogen interaction[29],

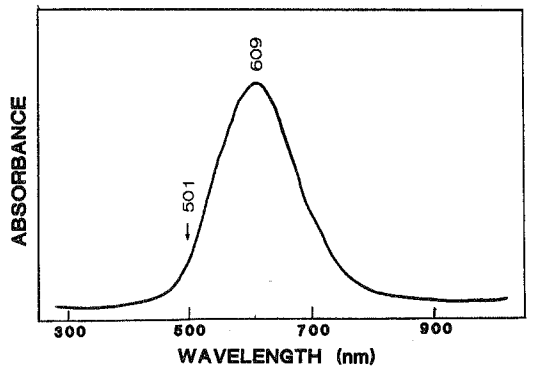

Fig. 7. Metal-to-metal charge transfer absorption for $(NC)_5Fe$–CN–$Os(NH_3)_5^{1-}$ in unbuffered water as solvent.

manifest here as an increase in ν^2_{Ru-N} with increasing donor number. For the higher frequency mode the dependence on the solvent is reversed and the explanation offered in Ref.[18] is more complex. Regardless of the details of the explanations, however, the Raman experiments clearly show that internal vibrational modes can be modulated by external interactions. We are currently exploring solvent effects in other chemical systems, most notably $Ru(bpy)_2(CN)_2$, which exhibits significant vibrational frequency shifts in response to solvent Lewis acidity variations.

BRIDGE ASSISTED (BRIDGE INHIBITED) METAL-TO-METAL CHARGE TRANSFER

A common theme in redox chemistry for both naturally-occurring and synthetically-assembled donors and acceptors is the facilitation of charge transfer by bridging ligands. Generally, these are thought to enhance electron transfer by lowering activation barriers and/or enhancing electronic coupling. The latter effect is especially important from our perspective because it leads to high absorbances for related *optical* electron transfer reactions[30] and therefore good enhancement of Raman scattering. In an earlier report we described a Raman investigation of bridge-assisted electron transfer in the system, $(NC)_5Ru^{II}$–CN–$Ru^{III}(NH_3)_5^{1-}$. Reported here are studies of a related system, $(NC)_5Fe^{II}$–CN–$Os^{III}(NH_3)_5^{1-}$:

$$(NC)^5Fe^{II}\text{–CN–}Os^{III}(NH_3)_5^{1-} \xrightarrow{h\nu} (NC)_5Fe^{III}\text{–CN–}Os^{II}(NH_3)_5^{1-}. \quad (15)$$

In the iron–osmium complex an intervalance absorption band of moderately high intensity exists with $\lambda_{max} = 609$ nm in water [Fig. 7; equation (15)]. Laser excitation at post-resonance (501.7 nm) leads to enhanced Raman scattering as shown in Fig. 8. (Enhancement was demonstrated by varying the excitation wavelength.) A key feature of the spectrum is that enhanced scattering is observed from both ends of the mixed-valence ion, based on a single electronic excitation. (This clearly identifies the transition as a metal-to-metal excitation.) For example, an ammine–osmium bending mode occurs at 267 cm^{-1} and cyanide stretching modes exist at 2103 (strong), 2062 (weak) and 2050 cm^{-1} (weak). (Splitting of the single depolarized C≡N stretch normally found in $M(CN)_6^{4-}$ species is an obvious chemical consequence of the symmetry lowering imposed by ligand bridging to osmium pentaammine.) By analogy with $(NC)_5Ru$–CN–$Ru(NH_3)_5^{1-}$ [18], the highest frequency stretch is assigned to the bridging cyanide. The bands at 2062 and 2050 cm^{-1} are assigned as radial and axial C≡N stretches, respectively.

Additional bands exist at 602 and 546 cm^{-1}, corresponding to a single band (585 cm^{-1}) assigned as the ν_7 mode in $Fe(CN)_6^{4-}$ [31]. This mode has been shown to contain both Fe–CN stretching and Fe–C≡N bending character[31]. On the basis of the shift to lower energy from that found for the monomer, the band at 546 cm^{-1} is assigned as a displacement associated with the bridge. (Electron withdrawal to form the bridging bond presumably reduces the

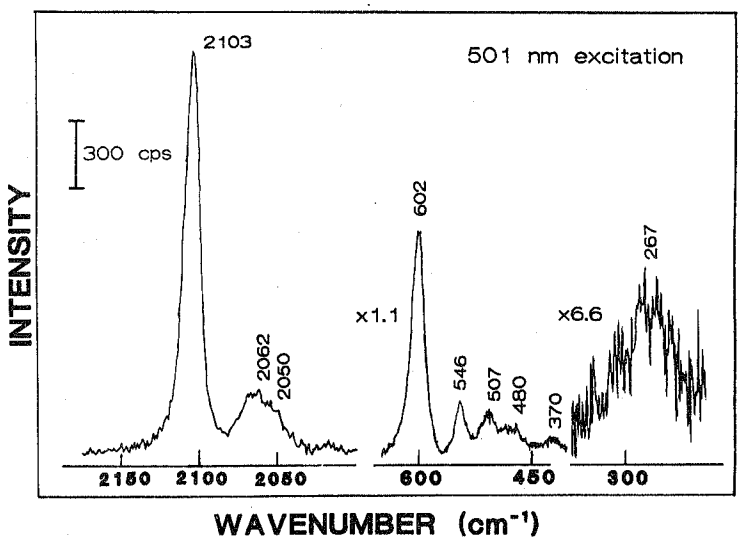

Fig. 8. Post-resonance Raman scattering from 40 mM $(NC)_5Fe$–CN–$Os(NH_3)_5^{1-}$ in H_2O based on 501.7 nm excitation.

Table 2. Structural and Franck–Condon charge transfer parameters for $(NC)_5Fe$–CN–$Os(NH_3)_5^{1-}$

Mode/ cm^{-1}	Relative intensity	$\lvert\Delta a\rvert$/Å	χ_i/cm^{-1}	Assignment
2103	5.0	0.044	810	$\nu_{C\equiv N}$ bridge
2062	2.4	0.009	130	$\nu_{C\equiv N}$ radial
2050	1.4	0.014	80	$\nu_{C\equiv N}$ axial
602	5.4	0.044	1020	ν_{Fe-C} terminal
456	1.0	0.043	210	ν_{Fe-C} bridge
507	0.85	0.028	190	ν_{Os-NH_3} radial
480	0.57	0.050	140	ν_{Os-NH_3} axial
370	0.20	0.035	60	ν_{Os-NC}
267	0.50	0.056	210	$\delta_{H_3N-Os-NH_3}$

ability to σ bond through the carbon atom, thereby yielding a decreased force constant for the vibration.) The higher energy band is assigned as either an axial (four bond) or terminal (five bond) Fe–CN stretching motion. The bands at 507 and 480 cm^{-1} are assigned to radial and axial Os–NH_3 stretches. Finally, the band at 370 cm^{-1} is tentatively ascribed to the Os–NC stretch.

Variations in intensity among the modes can be analyzed *via* time-dependent theory [equations (4), (9), (10) and (13)] to yield bond displacements and reorganizational energy components. The results of such an analysis are shown in Table 2. Comparison of Δa_{CN} (radial) for the iron–osmium complex (0.009 Å) with Δa_{CN} for $Fe(CN)_6^{4-/3-}$ (0.01 Å) suggests very good agreement between the scattering analysis and independent X-ray crystallographic measurements[32]. A comparison of Δa_{Fe-C} for the mixed-valance ion (0.043 Å) and $Fe(CN)_6^{4-/3-}$ (0.026 Å)[32] however, indicates only fair coincidence. We have remarked elsewhere[18] that solvent effects or other sources of absorption band broadening may lead to overestimates [*via* equation (10)] of bond length displacements in the scattering analysis. Further discussion and analysis of anomalous broadening effects can be found in reports by Champion and coworkers[33, 34]. Alternatively, the greater value of Δa_{Fe-C} for the mixed-valence species [equation (15)] might possibly reflect additional spectroscopic contributions from mixing with bending motions (see above); these of course would not appear in X-ray studies of monomeric model compounds.

Perhaps the most interesting finding in Fig. 8 is that a rather large number of modes (or types of bonds) participate in the vibrational activation of intramolecular electron transfer in $(NC)_5Fe$–CN–$Os(NH_3)_5^{1-}$. Worth noting in particular are the bridging modes (C≡N, Fe–CN, Ru–NC; Table 2) which comprise more than a third of the total vibrational barrier. In a vibrational sense, therefore, the cyanide bridge serves to inhibit rather than facilitate charge transfer. It is important to realize that these points (and others) would be difficult to establish by any conventional X-ray structural method (because of the short lifetime of $(NC)_5Fe^{III}$–CN–$Os^{II}(NH_3)_5^{1-}$) and that the Raman method appears, at present, to provide the only quantitative route to such information.

OUTER-SPHERE ELECTRON TRANSFER

The vast majority of electron transfer reactions involve outer-sphere rather than bridge-mediated reaction pathways. We have been interested, therefore, in discovering whether these types of reactions can be usefully investigated by the time-dependent scattering method. We describe here some very preliminary scattering experiments which suggest that quantitative vibrational structural studies are indeed possible for outer-sphere reactions.

The specific reaction examined was the one-electron reduction of 4-cyanomethylpyridinium:

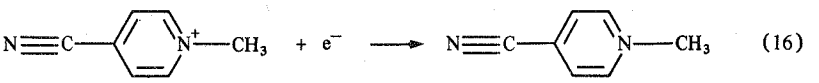

(16)

Reaction (16) is particularly interesting because, at electrode surfaces, it is chemically irreversible. (Product decomposition apparently occurs by a dimerization pathway[35].) This renders structural studies by conventional X-ray methods impossible, leaving Raman scattering as perhaps the only viable experimental methodology. To provide electronic and vibrational spectroscopic access, the cyanomethylpyridinium cation (NC–py-CH_3^+) was paired with iodide anion in acetonitrile as solvent. Because iodide is an excellent electron donor, the pairing gives rise to an outer-sphere charge transfer absorption band[36] centered at 428 nm ($\epsilon = 270\ M^{-1}\ cm^{-1}$). Unlike reaction (16), however, the optical charge transfer [equation (17)] is chemically (thermally) reversible. We note further that because the iodide ion is monatomic, any vibrational spectroscopic information will pertain exclusively to the NC–py-$CH_3^{+/0}$ redox couple.

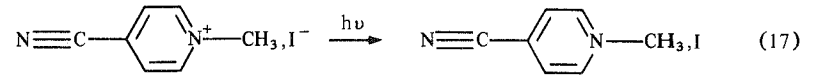

(17)

Figure 9 shows a Raman spectrum of NC–py-CH_3^+, I^- based on near resonant excitation (514.5 nm) with an argon ion source. Preliminary analysis indicates that at least 15 modes are active. Table 3 gives a listing along with very preliminary assignments. Two experiments were done to show that the scattering in Fig. 9 is resonantly enhanced: (1) spectra were recorded off resonance (647 nm excitation) and were found to be greatly diminished in intensity; (2) at 514.5 nm, spectra were recorded for both CN–py–CH_3^+, Cl^- and CN–py–CH_3^+, I^- (Fig. 10). The former is non-chromophoric at this wavelength due to the comparatively poor electron donating ability of chloride. As expected, scattering from the chloride salt is considerably diminished. Both experiments indicate, in fact, that nearly all of the modes listed in Table 3 are electronically enhanced,

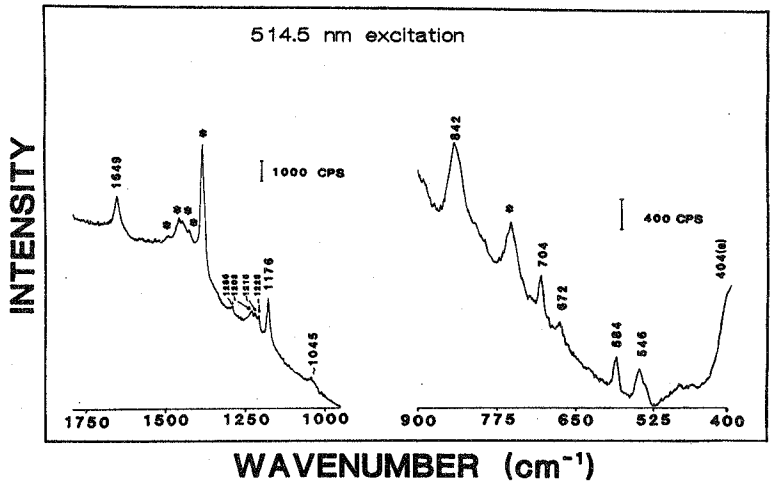

Fig. 9. Near-resonant Raman scattering spectrum of NC–py-CH_3^+, I^- in acetonitrile based on 514 nm excitation. The sloping background is due to sample or impurity fluorescence.

and that the enhancements amount to factors of five or more.

In principle, the data contained in Fig. 9 could be analyzed further to yield normal mode displacements, bond displacements, reorganizational energy components and so on. For a variety of reasons (chiefly relating to spectral quality, spectral corrections and the incompleteness of spectral assignments) we have not yet chosen to do so. The observation of outer-sphere charge-transfer enhancement, however, clearly indicates that time-dependent scattering methods will eventually be useful quantitative tools for monomeric redox structural studies.

Table 3. Vibrational frequencies and preliminary structural assignments for resonance enhanced Raman scattering from 4-cyanomethylpyridinium iodide

Frequency/cm^{-1}	Assignment†§
2250†	$\nu_{C\equiv N}$
1649	$\nu_{C=C}$
1286	ν_{C-C} (inter ring)
1228	π_{C-H}
1215	π_{C-H}
1203	π_{C-H}
1176	ν_{N-CH_3}
1045	π_{C-H}
842	$\nu_{N-CH_3} + \delta_{C-N-CH_3}$
704¶	?
672	δ_{C-N-CH_3}
584	?
546	?
404	δ_{C-C}
285	δ_{C-C}

*Determined in acetonitrile as solvent, except as noted.
†Determined in methylene chloride as solvent.
‡Preliminary vibrational assignments made on the basis of: (1) M. Forter, R. B. Girling and R. E. Hester *J. Raman Spectrosc.* **12,** 36 (1982); (2) E. Spinner, *Aust. J. Chem* **20,** 1805 (1967); (3) A. Benchenane, L. Bernard and T. Théophanides, *J. Raman Spectrosc.* **2,** 543 (1974).
§ν = stretch, δ = in-plane bend, π = out of plane bend.
¶Not detectably enhanced.

INTERFACIAL CHARGE TRANSFER

Obviously the electron transfer reactions of most interest to electrochemists are interfacial reactions. In principle, the time-dependent Raman scattering technique could be applied to interfacial reactions if surface-to-molecule or molecule-to-surface electronic

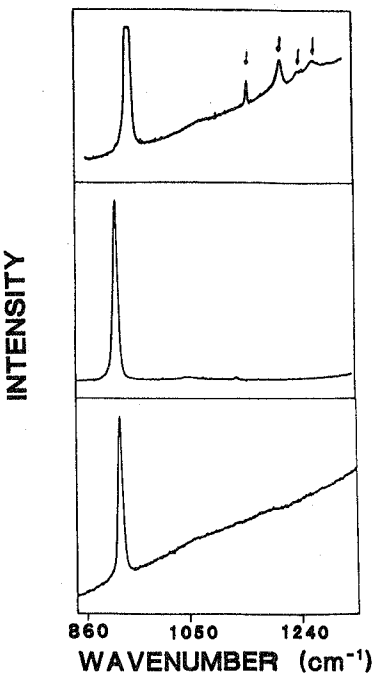

Fig. 10. Raman spectra for: 4-cyanomethylpyridium iodide in acetonitrile (top), acetonitrile only (middle), and 4-cyanomethylpyridium chloride (bottom). Excitation wavelength = 514 nm. Resonantly enhanced peaks (top spectrum) are labelled with arrows. (The large peak on the left hand side of each spectrum is due to a reference compound.)

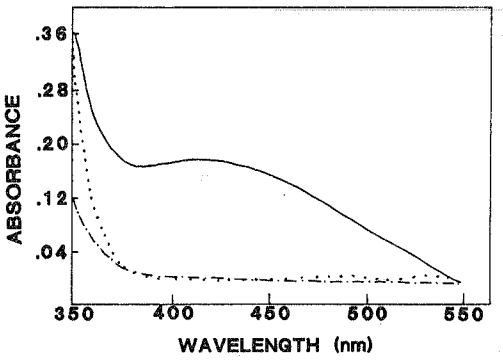

Fig. 11. Visible absorption spectra of $Fe(CN)_6^{4-}$/colloidal-TiO_2 sol (solid line), free $Fe(CN)_6^{4-}$ (dashed line) and free colloidal-TiO_2 sol (dotted line). Conditions are as follows: $Fe(CN)_6^{4-}$/colloidal-TiO_2 sol contains 0.01 mM $Fe(CN)_6^{4-}$ mixed with 1 g/L^{-1} colloidal-TiO_2, free $Fe(CN)_6^{4-}$ concentration is 0.83 mM, free colloidal-TiO_2 sol contains 0.75 g TiO_2 per liter of solution. The pH in all three experiments is 2.5.

transitions were available for resonant excitation. We wish to describe in this section two examples of interfacial vibrational structural investigations based on surface intervalence excitation.

The first reaction chosen was optical electron transfer from $Fe(CN)_6^{4-}$ to colloidal titanium dioxide:

Following Vrachnou and co-workers[37], we find that an intense optical absorption exists ($\lambda_{max} \approx 410$ nm, $\epsilon \approx 5000\ M^{-1}\,cm^{-1}$) for the "surface intervalence" charge transfer reaction in equation (1) (see Fig. 11; the colloid provides an exceptionally large surface area which greatly facilitates optical observation). We further find (Fig. 12) that Raman scattering spectra can be readily obtained based on near-resonant excitation (488 nm)[21]. Control experiments at 514.5 nm (nominally preresonant), at 647.1 nm (off resonance), with ferrocyanide alone, or with colloidal TiO_2 alone, all show the scattering in Fig. 12 to be resonantly enhanced (*eg* enhancement factors of at least 20 for the highest energy modes).

Table 4 lists the relative intensities, unitless normal coordinate displacements and bond-length changes obtained for resonance enhanced modes by application of equations (4) and (9). Absolute Δ and Δa values were derived by assuming that the changes in length for non-bridging Fe–C bonds equalled those determined crystallographically for free $Fe(CN)_6^{3-/4-}$ [32]. Mode assignments were made by analogy to $Fe(CN)_6^{4-}$ [38], $(H_3N)_5Ru$–NC–$Fe(CN)_5^{1-}$ [18], $(H_3N)_5Os$–NC–$Fe(CN)_5^{1-}$ and related systems[39], and will be described in greater detail elsewhere. From the table, a number of points are worth noting: (1) the total number of modes (or types of bonds) displaced is once again large (10), indicating that even the simplest of interfacial redox reactions may entail substantial complexity in vibrational activation; (2) as seen for related binuclear metal systems (in solution) [18, 39], bridging modes suffer the greatest displacement, with the C≡N bridging mode providing the largest single contribution to the vibrational barrier; (3) remarkably, three *surface* modes are enhanced and therefore displaced during optical electron transfer. This last observation is unprecedented experimentally and is at odds with most, if not all, existing theoretical views of interfacial electron transfer.

While the mode assignments in Table 4 are reasonably well established, questions do arise regarding the possibility of more than one type of binding geometry (*eg* doubly-bridged) and the degree of protonation of the bound ferrocyanide. We performed a number of control experiments where: (1)$Fe(CN)_6^{4-}$ and colloidal TiO_2 concentrations were substantially varied; (2) the

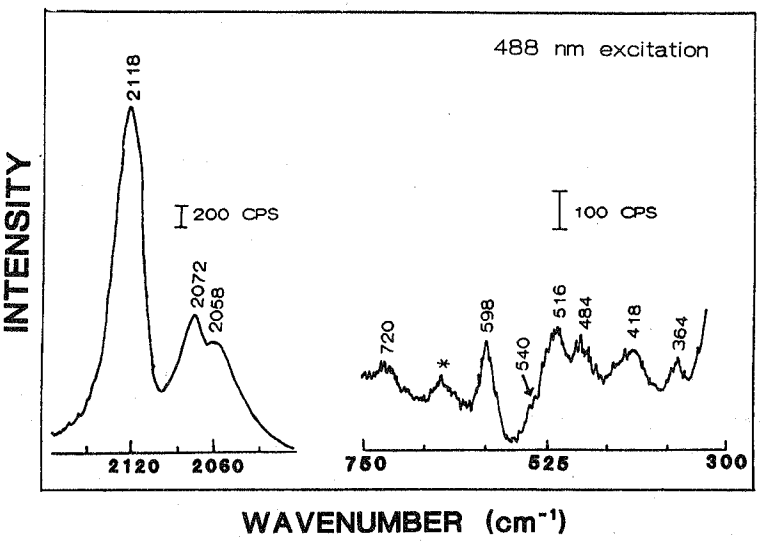

Fig. 12. Preresonance Raman spectrum of 0.6 mM $Fe(CN)_6^{4-}$/5.8 gL^{-1} TiO_2 colloid at pH = 2.0 based on 488 nm excitation. The asterisk at 656 cm^{-1} denotes an unenhanced E_g mode of TiO_2. The mode at 540 cm^{-1} is real and is more clearly resolved in experiments performed at 457.9 nm (from Ref.[21]).

Table 4. Spectroscopic, structural and reorganizational parameters for electron transfer from $Fe(CN)_6^{4-}$ to colloidal TiO_2

Mode/cm^{-1}	Relative intensity*†	Δ^2	$\lvert\Delta a\rvert$/Å	χ_i/cm^{-1}	Assignment
2118	20.0	0.95‡	0.048	1000	$\nu_{C\equiv N}$ bridge
2072	6.61	0.33	0.014	340	$\nu_{C\equiv N}$ radial
2058	5.44	0.27	0.026	280	$\nu_{C\equiv N}$ terminal
720	0.27	0.11	?	40	?
598	1.00	0.59	0.026§	180	ν_{Fe-C}
540	0.33	0.24	0.039	60	ν_{Fe-C} bridge
516	1.12	0.89	¶	230	ν_{TiO}
484	0.90	0.82	¶	200	ν_{TiO}
418	0.56	0.69	¶	140	ν_{TiO}
364	0.27	0.43	0.059	80	ν_{Ti-CN}

*Depolarization studies indicate that all modes, with the possible exception of modes at 540 and 720 cm^{-1} (too weak to determine with certainty), are totally symmetric.
†Within the experimental uncertainty, relative intensities are unaffected by changes in excitation wavelength.
‡All values scaled to the value for Δ^2 at 598 cm^{-1}.
§Taken from (or taken as) the crystallographically determined value[11] for $Fe(CN)_6^{4-/3-}$.
¶Value not determined, since the measured normal coordinate displacement (Δ) may entail more than one type of bond length displacement (*ie* local-mode approximation may not be appropriate).

pH was varied between 1 and 3; (3) multiple excitation wavelengths were used in resonance; (4) an isotope study using a 7:1 dilution in D_2SO_4/D_2O was completed. Interestingly, all of these experiments led to no change in relative Raman intensities or frequency shifts. These results, therefore, tend to support the notion that only one type of complexed ferrocyanide species exists, which apparently is unprotonated, and is bound to titanium *via* a single-cyanide ligand. Additional concerns relating to possible competitive scattering from Prussian blue or titanate/$Fe(CN)_6^{4-}$ species have been considered and successfully eliminated; experimental details and discussion are given elsewhere[21].

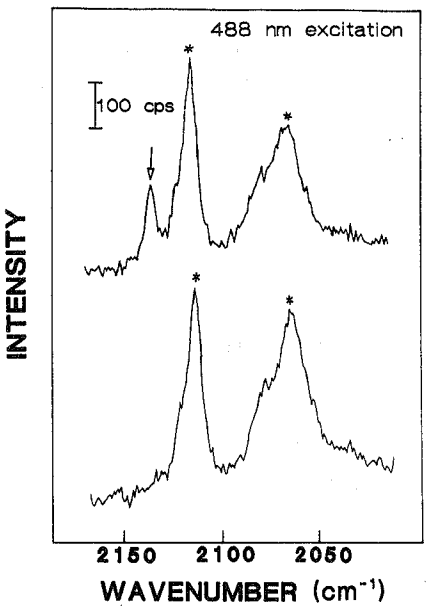

Fig. 13. Potential dependence of Raman scattering from TiO_2 in contact with $Os(CN)_6^{4-}$ in water at pH = 2. Peaks at 2063 and 2115 cm^{-1} (marked with asterisks) are associated with $Os(CN)_6^{4-}$ in solution. Upper spectrum: +0.8 V; lower spectrum: −0.5 V *vs sce* reference. Spectra are offset vertically for clarity.

In order to extend the study to a more authentically "electrochemical" environment, we replaced the titanium dioxide colloid with a bulk titanium rod containing an anatase overlayer. The method of overlayer preparation largely followed that of Vlachopoulos *et al.*[40]. The molecular reactant at this surface was $Os(CN)_6^{4-}$; like ferrocyanide on the colloid surface (Fig. 10) the osmium species displays a visible region electronic absorption corresponding to interfacial charge transfer[37].

Raman spectra for this system were collected in a thin-layer configuration, where the thin-layer solution contained excess $Os(CN)_6^{4-}$. Figure 13 shows the results of a resonance experiment (488 nm excitation). The top spectrum was obtained with the electrode held at +0.8V *vs sce* reference. Cyanide stretching for both solution (2063 and 2115 cm^{-1}, non-resonant) and surface-bound (2136 cm^{-1}, resonant) $Os(CN)_6^{4-}$ species is observed. The bottom spectrum was obtained at −0.5 V. Here only the solution species is seen. Our interpretation is that polarization at −0.5 V fills the anatase conduction band, renders the electrode conductive, and eliminates the Ti(IV) entity (*ie* electron acceptor) required for surface intervalence charge transfer. In the absence of a surface intervalence absorption band, Raman scattering is greatly diminished because a mechanism for resonance enhancement is no longer present.

Current work is aimed at extending the electrochemical Raman studies beyond the cyanide stretching region, exploring more thoroughly the potential dependence, identifying more accurately the locations of semiconductor band edges and the formal potentials of adsorbates, evaluating pH effects and evaluating the dependence of scattering intensity on excitation wavelength. It is hoped that the technique will prove generally useful in the study of interfacial electron transfer at semiconductors and that eventually it may be extended to metal electrode surfaces.

Acknowledgements—This research was supported by the U.S. Department of Energy, Office of Energy Research, Division of Chemical Sciences (Grant No. DE-FG02-87ER13808) and by the Office of Naval Research. We thank Professor Jeanne Pemberton, Mr Mark Bryant and Mr Ray Sobocinski of the University of Arizona for assistance and collaboration on the experiment shown in Fig. 10. A portion of the Raman instrumentation at Northwestern is maintained by the Materials Research Center (NSF-DMR-8821571). The remaining instrumentation was acquired with the generous assistance of the Department of Energy and the Northwestern University Research Grants Committee. JTH acknowledges a fellowship from the Alfred P. Sloan Foundation.

REFERENCES

1. P. George and J. S. Griffith, in *The Enzymes* (Edited by P. D. Boyer, H. Lardy and K. Myrback). Academic Press, New York (1959).
2. R. A. Marcus, *J. chem. Phys.* **43,** 1261 (1965).
3. N. Sutin, *Prog. inorg. Chem.* **30,** 441 (1983).
4. B. S. Brunschwig, C. Creutz, D. Macartney, T. K. Sham and N. Sutin, *Faraday Discuss. chem. Soc.* **74,** 113 (1982).
5. H. D. Abruña, J. H. White, G. Albarelli, M. Bommarito, M. J. Bedzyk and M. McMillan, *J. phys. Chem.* **92,** 7045 (1988).
6. D. Tannor and E. J. Heller, *J. chem. Phys.* **77,** 202 (1982).
7. E. J. Heller, *Accs Chem. Res.* **14,** 368 (1981).
8. E. J. Heller, R. L. Sundberg and D. Tannor, *J. phys. Chem.* **86,** 1822 (1982).
9. D. E. Morris and W. H. Woodruff, *J. phys. Chem.* **89,** 5795 (1985).
10. A. B. Myers and R. A. Mathies, in *Biological Applications of Raman Spectroscopy* (Edited by T. G. Spiro) Vol. 2. John Wiley, New York (1988).
11. P. M. Champion, in *Biological Applications of Raman Spectroscopy* (Edited by T. G. Spiro), Vol. 3. John Wiley, New York (1988).
12. M. O. Truhlson, G. D. Dollinger and R. A. Mathies, *J. Am. chem. Soc.* **109,** 587 (1987).
13. L. Tutt and J. I. Zink, *J. Am. chem. Soc.* **108,** 5830 (1986).
14. Y. Y. Yang and J. I. Zink, *J. Am. chem. Soc.* **107,** 4799 (1986).
15. L. Tutt, D. Tannor, J. Schindler, E. J. Heller and J. I. Zink, *J. phys. Chem.* **87,** 3017 (1983).
16. K.-S. Shin, R. J. H. Clark and J. I. Zink, *J. Am. chem. Soc.* **111,** 4244 (1989).
17. K.-S. Shin and J. I. Zink, *J. Am. chem. Soc.* **112,** 7148 (1990).
18. S. K. Doorn and J. T. Hupp, *J. Am. chem. Soc.* **111,** 4704 (1989).
19. S. K. Doorn and J. T. Hupp, *J. Am. chem. Soc.* **111,** 1142 (1989).
20. R. L. Blackbourn, S. K. Doorn, J. A. Roberts and J. T. Hupp, *Langmuir* **5,** 696 (1989).
21. R. L. Blackbourn, C. S. Johnson and J. T. Hupp, *J. Am. chem. Soc.* **113,** 1060 (1991).
22. K. T. Schomacker and P. M. Champion, *J. chem. Phys.* **90,** 5982 (1989).
23. T. J. Meyer, *Pure appl. Chem.* **58,** 1193 (1986).
24. G. W. Robinson and R. P. Frosch, *J. chem. Phys.* **38,** 1187 (1963).
25. W. Siebrand and D. F. Williams, *J. chem. Phys.* **46,** 403 (1967).
26. J. V. Casper, T. D. Westmoreland, G. H. Allen, P. G. Bradley, T. J. Meyer and W. H. Woodruff, *J. Am. chem. Soc.* **106,** 3492 (1984).
27. R. M. Badger, *Phys. Rev.* **48,** 284 (1935).
28. V. Gutman, *Electrochim. Acta* **21,** 661 (1976).
29. J. C. Curtis, B. P. Sullivan and T. J. Meyer, *Inorg. Chem.* **22,** 224 (1983).
30. C.Creutz, *Prog. inorg. Chem.* **30,** 1 (1983).
31. W. P. Griffith and G. T. Turner, *J. chem. Soc. A* 858 (1970).
32. B. I. Swanson, S. I. Hamburg and R. R. Ryan, *Inorg. Chem.* **13,** 1685 (1974).
33. K. T. Schomacker and P. M. Champion, *J. chem. Phys.* **84,** 5314 (1986).
34. V. Srajer, K. T. Schomacker and P. M. Champion, *Phys. Rev. Lett.* **57,** 1267 (1986).
35. I. Carelli, *Electrochim. Acta* **35,** 1185 (1990).
36. E. M. Kowsower, *J. Am. chem. Soc.* **80,** 3253 (1958).
37. E. Vrachnou, M. Grätzel and A. J. McEvoy, *J. electroanal. Chem.* **258,** 193 (1989).
38. L. H. Jones, M. N. Memering and B. I. Swanson, *J. chem. Phys.* **54,** 4666 (1971).
39. S. K. Doorn, Ph.D. Dissertation, Northwestern University (1990).
40. N. Vlachopoulos, P. Liska, J. Augustynski and M. Grätzel, *J. Am. chem. Soc.* **110,** 1216 (1988).